catalysts

MDPI

Article

Natural Polymer-Based Iron Oxide (Fe_3O_4) Synthesis, Characterization and Its Application for 1-Amino-Nitrobenzene Degradation in Assistance with Oxidants

Jayachandrabal Balachandramohan [1], Mithun Kumar [1], Thirugnanasambandam Sivasankar [1,*] and Manickam Sivakumar [2]

[1] Department of Chemical Engineering, National Institute of Technology, Tiruchirappalli 620 015, TamilNadu, India
[2] Petroleum and Chemical Engineering, Faculty of Engineering, Universiti Teknologi Brunei, Bandar Seri Begawan BE1410, Brunei
* Correspondence: ssankar@nitt.edu; Tel.: +91-431-2503131

Abstract: A natural polymer-based iron oxide (Fe_3O_4) nanocomposite was prepared through a sonochemical-assisted precipitation method. Characterization studies such as X-ray diffractometer, scanning electron microscopy, and transmission electron microscopy have revealed that the synthesized nanocomposites are homogenously distributed, having an average size of ~49 nm with a cubical spinel structure. The toxic 1-amino-nitrobenzene was initially treated with a sonophotochemical process in the presence of synthesized nanocomposites, resulting in lower efficiency, whereas with the addition of oxidants, the efficiency enhanced significantly. The parametric effects with respect to the initial solution pH, nanocomposites dose, 1-amino-nitrobenzene concentration, and oxidant concentration were studied, and it was found that an approximately 75% removal efficiency of 1-amino-nitrobenzene was achieved within 120 min. Further, the performance of the catalyst on the oxidation of 1-amino-nitrobenzene with sodium persulfate was also investigated, and it was found that a 95% removal efficiency was attained.

Keywords: ferroferric oxide-guaran nanocomposite; encapsulation; ultrasound; 1-amino-nitrobenzene; photocatalytic oxidation

check for updates

Citation: Balachandramohan, J.; Kumar, M.; Sivasankar, T.; Sivakumar, M. Natural Polymer-Based Iron Oxide (Fe_3O_4) Synthesis, Characterization and Its Application for 1-Amino-Nitrobenzene Degradation in Assistance with Oxidants. *Catalysts* **2022**, *12*, 1161. https://doi.org/10.3390/catal12101161

Academic Editors: Guan-Ting Pan, Siewhui Chong and Timm Joyce Tiong

Received: 29 July 2022
Accepted: 23 September 2022
Published: 2 October 2022

Publisher's Note: MDPI stays neutral with regard to jurisdictional claims in published maps and institutional affiliations.

Copyright: © 2022 by the authors. Licensee MDPI, Basel, Switzerland. This article is an open access article distributed under the terms and conditions of the Creative Commons Attribution (CC BY) license (https://creativecommons.org/licenses/by/4.0/).

1. Introduction

Amines and their derivatives have found an important place for their use, specifically in the pharmaceutical, chemical, and biological industries. They are notably used as antioxidants, and also for the production of different types of dyes, pesticides, intermediate pharmaceutical products, etc. [1–3]. In specific, 1-amino-nitrobenzene (ANB) has been used for the production of several vital compounds, not limited to dyes, antioxidants, pesticides, and medicines. They are non-biodegradable, highly stable, and toxic in water when found at lower levels, which affects their aquatic lifecycle and, indeed, human health [4–7].

Different treatment methods have been adopted for ANB removal from aqueous solutions, i.e., physical, chemical, and biological methods [8,9]; these include hydrothermal decomposition [10], Fenton oxidation [11], photocatalytic degradation [12], biodegradation [13], adsorption [14], and others [4]. In the physical methods such as carbon fiber [15] and carboxylate polymeric matrix absorptions [14], mineralization could not be achieved as the pollutant changes from one form to another, and further treatment was required. Whereas hydrothermal decomposition [10] and photocatalytic degradation suffer from high capital and operating cost [6,11,16–18], ANB was found to be resistant to biological degradation [6], which is due to the nitro group that is attached to the aromatic ring providing the required stability to ANB. This stable nature is reflected in its lower degradation

rate and leads to the formation of carcinogenic intermediate compounds such as nitroso and hydroxyl amines [4,13].

In recent decades, advanced oxidation processes (AOPs) have been extensively used and studied to degrade and mineralize sturdy organic pollutants that are found difficult to treat using either biological or physicochemical processes. The sonochemical process is one of a kind, and it involves the formation of acoustic cavitation in which the heat generated from the cavity implosion generates highly reactive hydrogen atoms (H^+), hydroxyl radicals ($^\bullet OH$), hydrogen peroxide (H_2O_2), and molecular hydrogen (H_2) [19]. The sonochemical process influences both the oxidation and reduction reaction, which, in turn, increases the mineralization rate of the pollutant molecule [20–22]. At the same time, when catalysts are used, they activate the catalyst surface by particle fragmentation, and deagglomerate the catalyst, thereby decreasing the mass transfer limitations [23]. Among the treatment methods, heterogeneous Fenton-like systems are found suitable for the effective degradation of organic compounds [24–26]. Han et al. [26] showed that the Au/hydroxyapatite catalyst alongside a peroxidant can provide high activity and potential in eradicating the organic pollutant in full. The reaction occurs mainly through the decomposition of H_2O_2 into hydroxyl ($^\bullet OH$) and hydroperoxyl radicals ($HO_2^\bullet$) in the presence of a catalyst. Depending on the catalyst used, the degradation efficiency varies; for example, Zelmanov and Semiat [27] used Fe_3O_4 nanoparticles to gain higher efficiency for the treatment of ethylene glycol and phenol.

Recent studies on the degradation of ANB by photocatalysis [12], the Fenton oxidation process [11], oxidative decomposition by solar photo-Fenton AOPs [5], transient and steady-state photolysis [6,28], and oxidation of persulfate/Fe_3O_4 [29] have shown that the degradation of ANB was not economical on an industrial scale because of the high energy consumption of electrical lamps, high capital costs, and operating costs. Therefore, the intent of this work is to synthesize a Ferroferric oxide-guaran nanocomposite (FFGN) by the sonochemical precipitation method. It has been reported that Fe_3O_4 and its composites have potential application as a catalyst for photocatalytic degradation and as a sensor material, adsorbent, supercapacitor electrode, in lithium-ion batteries, and so on, due to its low-cost synthesis, no secondary pollution, *n*-type semiconducting behavior, and having a bandgap of Eg = 2.1 eV [30]. Different polymer materials could be used over metals/metal oxides to enhance their activity. For example, a detection limit of 1 ppb was possible for both polysaccharide-based gold–silver nanoparticles in the sensing of ammonia at room temperature [31,32]. Das et al., 2015 [33] synthesized a highly stable monodispersed silver nanoparticle in the presence of a blend of a polysaccharide (guar gum), which played a vital role in the long-term stabilization of the aqueous dispersions of silver nanoparticles. The aqueous dispersions of silver nanoparticles also displayed strong antibacterial and antioxidant properties. Impregnation of zerovalent iron (ZVI) onto the guar gum cross-linked soya lecithin nanocomposite hydrogel, synthesized via the ultrasonication method, enhanced the photodegradation of methyl violet by Sharma et al., 2019 [34]. Guaran was chosen as it controls the stability of the inorganic nanoparticles and is cost-effective owing to it being non-toxic, eco-friendly, readily available, and easy to manufacture by extraction, with less environmental impact [35,36]. Guaran has strong hydrogen bonding susceptibility in water, which stabilizes the synthesized metal NPs by acting as an excellent and better surface capping agent than starch and alginate, and its implicit biocompatibility and biodegradability makes it a potential alternative able to be used widely in a variety of applications in biotechnology and in environmental protection [37–39]. The synthesized nanocomposites were used to explore the heterogeneous Fenton-like system using ultrasound and photolysis as an advanced oxidation process in the presence of oxidizing agents for the degradation of ANB in an aqueous solution. The effects of parameters on the degradation of ANB such as FFGN concentration, initial solution pH, ANB concentration, and different oxidant concentrations were investigated. Finally, the sulfate radicals generated from persulfate activated by FFGN were anticipated to provide an environmentally friendly and highly efficient catalytic oxidation process for

aqueous ANB degradation. The mechanism of persulfate activation and ANB oxidation was elucidated, and the reusability of the catalyst was also explored.

2. Results and Discussion

2.1. Characterization of Synthetic Ferroferric Oxide-Guaran Nanocomposite

The X-ray diffraction pattern of the FFGN sample is shown in Figure 1A. The characteristic peaks were indexed at 30.1°, 35.4°, 43.0°, 53.39°, 56.9°, and 62.6°, corresponding to the diffraction planes of (220), (311), (400), (422), (511), and (440). The obtained peaks are in good agreement with standard ferroferric oxide of JCPDS card No. 00-019-0629. The peaks were characterized by cubic inverse spinel structure including the angles (2θ) that correspond to guaran at 28.5°, 29.5°, 34.1°, 38.6°, and 49.6° [40]. Hence, the presence of guaran and ferroferric oxide were evidenced. The zeta potential of the nanocomposite obtained from electrophoretic mobility is presented in Figure 1B. The polydispersity index (PDI) at 0.651 of FFGN was uniformly distributed with a zeta potential of -34.8 ± 0.3 mV, whereas, for ferroferric oxide, the PDI was 0.751 with a zeta potential of -16.6 ± 0.3 mV [30]. Due to the large negativity of the zeta potential, the particles were with minimal agglomeration. This was contemplated for achieving lower particle sizes and higher stability of the nanocomposites [41]. Hence, it could be said that the formed FFGN is highly stable and does not undergo agglomeration.

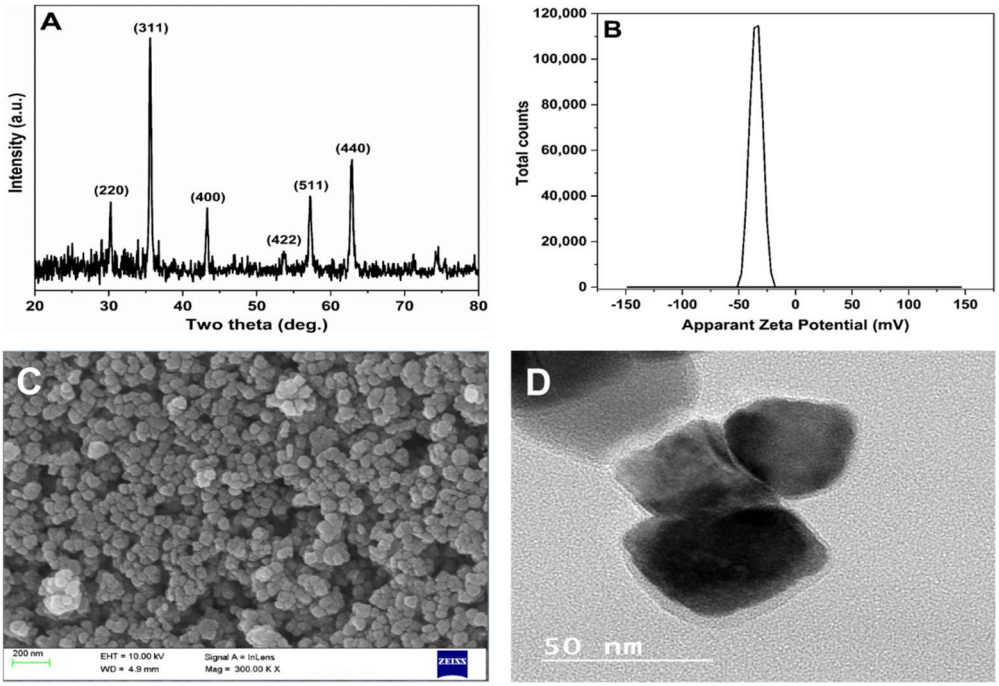

Figure 1. Characterization of FFGN (**A**) XRD, (**B**) Zeta potential, (**C**) SEM, (**D**) TEM.

The structural morphology of the FFGN is shown in Figure 1C,D. The SEM images impart that the particles are cubical in shape. The FFGN possesses good dispersion and there was no/minimal aggregation of particles due to the presence of guaran, thereby weakening the magnetic attraction among the iron particles. The image in Figure 1C shows that the ferroferric oxide was surrounded by guaran polymers or ferroferric oxide-guaran core/shell-like structure. The formation of the guaran polymer networks was due to the electrostatic and steric effects, and the •OH group of the galactose and mannose molecules further improve the stabilization of FFGN [42–44]. Figure 1D shows the TEM image of the as-prepared FFGN with a better crystalline structure. Polysaccharides such as guaran are promising O-providers and are highly reactive in the presence of high oxygen content. Guaran is a greener and more viable option in place of commonly used surfactants and

additives that are manufactured in the petrochemical industries [45,46]. The polysaccharide guaran acts as a capping agent, and the hydroxyl groups of the polymeric chain networks surround and protect the particles over long periods.

2.2. Sonophotochemical Degradation of ANB

Initially, the sonophotochemical degradation of ANB that was performed at solution pH 8.0 resulted in only a 13% removal, and when performed at pH 3.0, this had increased to 33%. In the presence of the FFGN catalyst at pH 3.0, the removal resulted in a 47% increase, which was due to the Fe^{2+} ions and OH groups present in the nanocomposite, which led to a lower pH condition [11].

2.2.1. Effect of Initial Solution pH

The pH of the reaction solution for the oxidative degradation of organic pollutants is a crucial parameter for Fenton's reaction, and, accordingly, the number of the $^{\bullet}OH$ radical generation varies. Figure 2 shows the effect of the initial solution pH on the sonochemical degradation of ANB in an aqueous solution. It was observed that the degradation efficiency of ANB declined from 47% to 4% and from pH 3.0 to 8.0. At an alkaline pH, the oxidation efficiency of FFGN decreases due to the formation of $Fe(OH)_3$, which reacts with H_2O_2 to form ferrous iron. At pH < 4.0, the formation of $Fe(OOH)^{2+}$ will be more due to the high concentration of hydrogen ions, and this increases the formation of $^{\bullet}OH$ radicals in the Fenton oxidation process [47]. It was observed that higher degradation was obtained at pH 3.0, in acidic conditions, which favor the dissolution of Fe, and large quantities of Fe^{2+} can be generated under acidic conditions. Fe^{2+}, along with H_2O, generates higher reactive $^{\bullet}OH$ radicals, playing an important role in disintegrating the sturdy ANB molecules [12]. The pH was considered to be optimum at pH 2.0–4.0, and the degradation of ANB was possible at pH 3.0 in an acidic medium, which prevents the catalyst iron from precipitating. Moreover, at pH < 3.0, due to the formation of a hexaaquairon ion, which lowers the available iron to react with H_2O_2, resulting in the stable formation of H_2O_2. At low pH, H^+ acts as a scavenger, resulting in the formation of oxonium ions $[H_3O_2]^+$, which reduces the reactivity of iron and retards the reaction. At pH > 4.0, the degradation declines, which is attributed to the ferrous and ferric hydroxide complex formation, which possesses Fe^{2+} in terms of OH radical production. The formation of ferric hydroxide, thus, removes the iron from the reaction and reduces the efficiency of the process. At an alkaline pH, the oxidation efficiency of FFGN decreases due to the formation of $Fe(OH)_3$, which reacts with H_2O_2 to form ferrous iron, and ferric hydroxide will precipitate, and both will result in a decrease in the efficiency of the Fenton process [48,49]. At pH > 4.0, the degradation declined, which was attributed to the ferrous and ferric hydroxide complex formation, which possesses Fe^{2+} in terms of OH radical production [11].

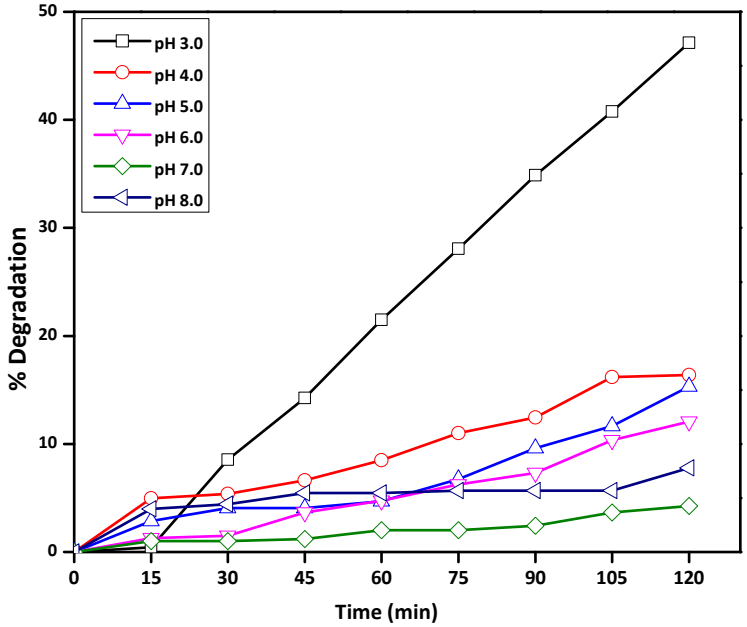

Figure 2. Degradation of ANB at different initial solution pH (FFGN = 0.5 g/L, ANB = 50 ppm, Amplitude = 40%, Probe = 25 mm, T = 25 ± 1 °C).

2.2.2. Effect of FFGN Concentration

The catalytic activity of FFGN toward ANB degradation was examined, and the experimental results are shown in Figure 3.

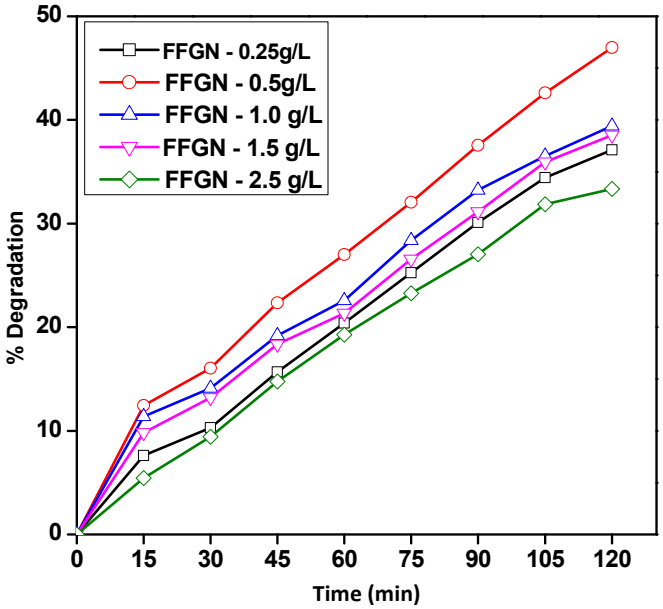

Figure 3. Degradation of ANB at different FFGN concentrations (pH = 3.0 ± 0.2, ANB = 50 ppm, Amplitude = 40%, Probe = 25 mm, T = 25 ± 1 °C).

The catalytic oxidation of ANB was performed by varying the FFGN dose from 0.25 to 2.5 g/L. Since better removal was obtained at pH = 3.0, this study was performed with pH = 3 ± 0.2, ANB = 50 ppm, and T = 25 ± 1 °C. The ANB degradation increased from 37% to 47% in the catalyst concentration variation study. When the FFGN content was 0.5 g/L, the ANB oxidation rate was at the highest level (i.e., 47%). As mentioned earlier, the Fe^{2+} dosage has a high impact on the disintegration of ANB through •OH radicals formed out of it. At an acidic pH, the •OH radical can be generated from a heterogeneous

reaction between the catalyst surface Fe^{II} ($\equiv Fe^{III}$) and H_2O_2 (Equation (1)) and from the outer-surface reaction between Fe^{2+} and H_2O_2, which cleaves the homolytic O-O bond, which was induced by the homogenous Fenton reaction by leached iron [26]. In addition, the guaran present in the surface of the nanocomposite also induces the Fenton oxidation process by producing the $^{\bullet}OH$ radical.

$$\equiv Fe^{II} + H_2O_2 \rightarrow \equiv Fe^{III} + OH^- + HO^{\bullet} \quad (1)$$

2.2.3. Effect of $NaIO_4$ Concentration

Even with an acidic pH and an iron catalyst, the removal obtained was relatively less and further enhancement was found to be essential. Hence, to improve the treatment efficiency of ANB, the aqueous medium was supplemented with the addition of $NaIO_4$ oxidant. The effect of varying concentrations (0.002 to 0.02 mol/L) of $NaIO_4$ on ANB degradation was performed at the experimental conditions of pH = 3.0 ± 0.2, ANB = 50 ppm, FFGN = 0.5 g/L, and T = 25 ± 1 °C, and the results are shown in Figure 4. The degradation of ANB varied from 52% to 45%, and the degradation rate decreased with the increase in the oxidant concentration. Clearly, the oxidant addition influenced the degradation rate more than with a mere catalyst where the degradation was 47%, and with oxidant addition, it could increase to 52%. The maximum degradation was observed for the oxidant concentration of 0.002 mol/L. The degradation of ANB decreases with the increase in $NaIO_4$ concentration, which was due to $^{\bullet}OH$ radical scavenging and the generation of $HO_2^{\bullet}$ radicals [26]. It could be concluded that the concentration of $NaIO_4$ has no considerable effect on ANB removal.

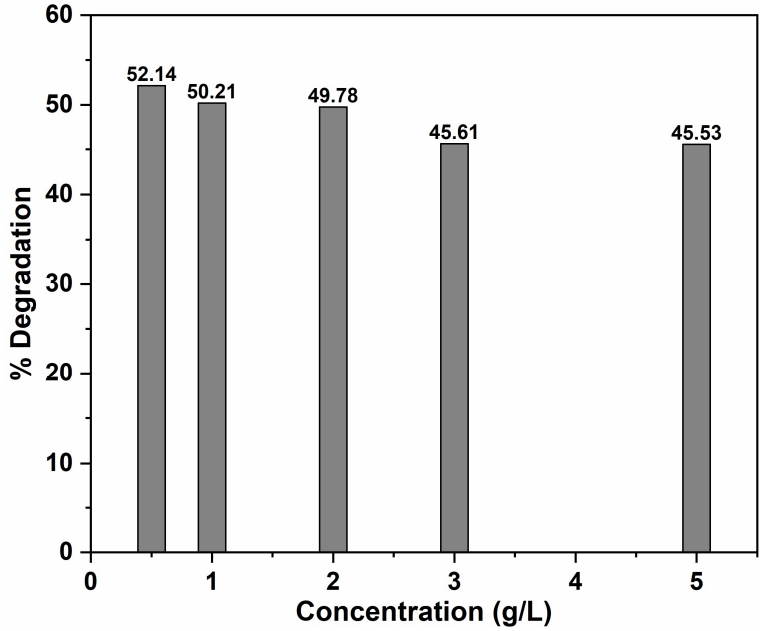

Figure 4. Degradation of ANB at different $NaIO_4$ concentrations (pH = 3.0 ± 0.2, FFGN = 0.5 g/L, ANB = 50 ppm, Amplitude = 40%, Probe = 25 mm, T = 25 ± 1 °C).

2.2.4. Mechanism of ANB Degradation by Sodium Periodate

Figure 5 represents the probable mechanism for the catalytic oxidation of ANB by FFGN nanocomposites. The catalytic oxidation of ANB by FFGN nanocomposites depends mainly on the addition of periodate, which generates very strong radicals such as $^{\bullet}OH$, $IO_4^{\bullet}$, $IO_3^{\bullet}$, and IO_3 as a result of periodate activation at an acidic pH [50]. In the oxidation process, sodium periodate can produce $IO_4^{\bullet}$ and $IO_3^{\bullet}$ radicals. $^{\bullet}OH$ and O_3 are also

generated during the activation process. $IO_4^{\bullet}$ and $IO_3^{\bullet}$ radicals can be reduced to periodate in the presence of O_3 according to the following equations [51,52].

$$O_3 + IO_3^{\bullet} \rightarrow IO_4^{\bullet} + O_2 \quad (2)$$

$$2IO_4^{\bullet} \leftrightarrow I_2O_8 \quad (3)$$

$$I_2O_8 + H_2O \rightarrow IO_3^- + IO_4^- + 2H^+ + O_2 \quad (4)$$

$$2IO_3^{\bullet} \leftrightarrow I_2O_6 \quad (5)$$

$$I_2O_6 + H_2O \rightarrow IO_4^- + IO_3^- + 2H^+ \quad (6)$$

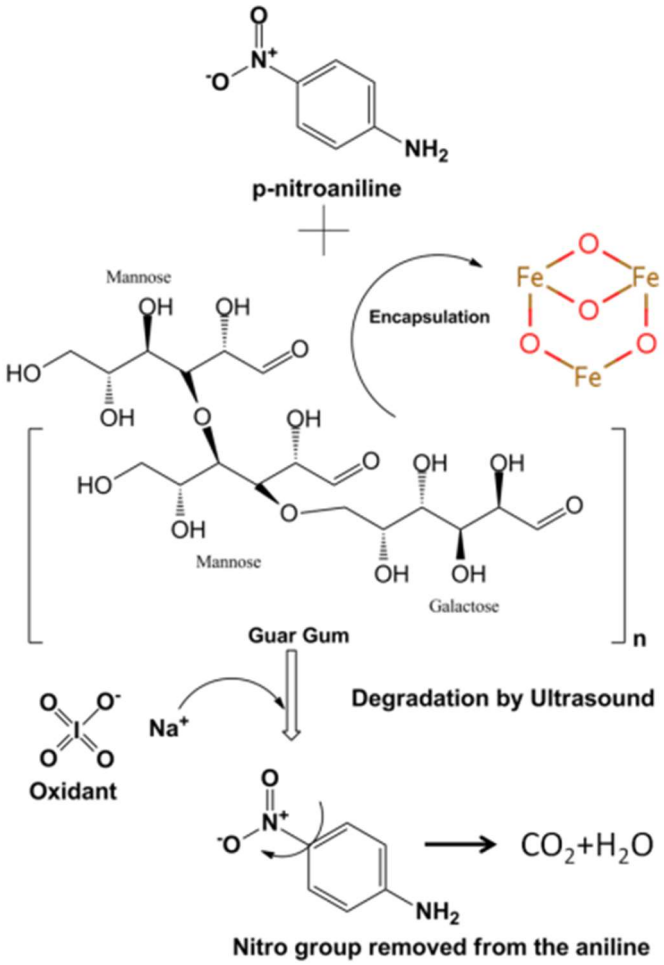

Figure 5. Proposed mechanism of the catalytic oxidation of ANB by FFGN.

The degradation of ANB happens in two stages: the first stage is the breakage of the benzene rings, and the second stage is the oxidation of the chain organic compound. The $^{\bullet}OH$, $IO_4^{\bullet}$, $IO_3^{\bullet}$, and IO_3 can destroy the benzene rings and finally convert them into H_2O and CO_2.

2.2.5. Effect of FFGN with Fixed $NaIO_4$ Concentration

Figure 6 shows the effect of the FFGN dose on ANB degradation by varying the FFGN concentration (0.5 to 10.0 g/L) at the experimental conditions of pH = 3.0 ± 0.2, ANB = 50 ppm, $NaIO_4$ = 0.002 mol/L, and T = 25 ± 1 °C. The degradation increased up to 75% with the increase in the FFGN concentration, and this was due to increased Fe^{2+} ions leading to the higher decomposition of H_2O_2 into $^{\bullet}OH$ radicals in the form of the Fenton reaction. However, the use of too high a concentration of Fe^{2+} leads to the formation of

ferric-based sludge. The ferric-based sludge complicates ANB degradation, which needs further treatment and disposal of the sludge. So, the concentration of the catalyst was a fixed constant of 0.5 g/L in order to avoid the formation of ferric-based sludge. The ANB degradation was investigated with different oxidants such as $Na_2S_2O_8$, H_2O_2, and Na_2SO_3 concerning the catalytic performance of FFGN for the catalytic oxidation of ANB.

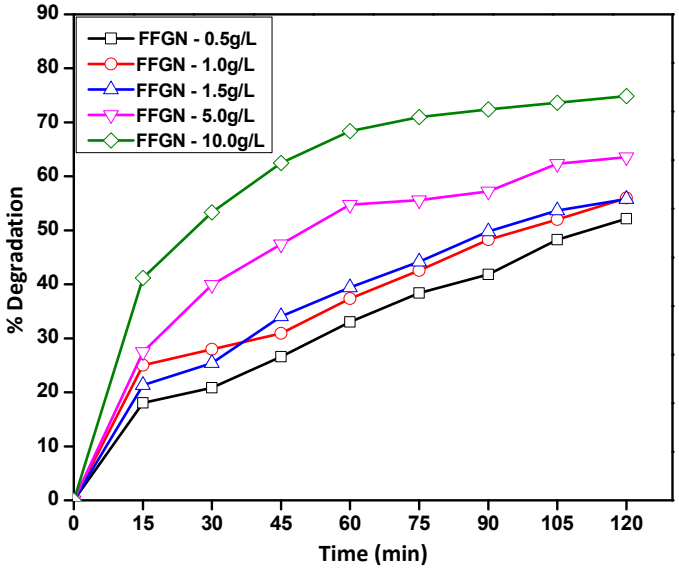

Figure 6. Degradation of ANB at different FFGN concentrations (pH = 3.0 ± 0.2, ANB = 50 ppm, $NaIO_4$ = 0.002 mol/L, Amplitude = 40%, Probe = 25 mm, T = 25 ± 1 °C).

2.2.6. Effect of FFGN with Different Oxidants

The effect of different oxidants on the degradation of ANB was performed at the experimental conditions of pH = 3.0 ± 0.2, ANB = 50 ppm, FFGN = 0.5 g/L, T = 25 ± 1 °C, and the results are shown in Figure 7.

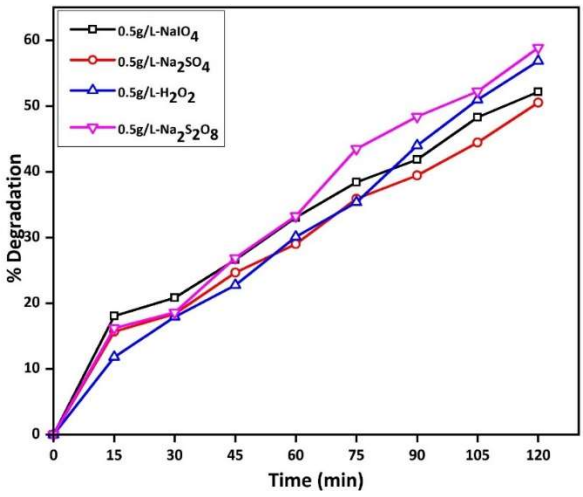

Figure 7. Degradation of ANB with different oxidants (pH = 3.0 ± 0.2, ANB = 50 ppm, FFGN = 0.5 g/L, Amplitude = 40%, Probe = 25 mm, T = 25 ± 1 °C).

The ANB removal varied from 52% to 58% for different oxidants such as sodium periodate ($NaIO_4$), sodium sulfate (Na_2SO_4), hydrogen peroxide (H_2O_2), and sodium persulfate ($Na_2S_2O_8$). The effect of the catalytic oxidation of ANB in the presence of sodium sulfate was found to be 50% as compared to $NaIO_4$ at 52%. Sodium sulfate forms Na^+ and SO_4^{2-} ions electrostatically, and SO_4^{2-} ions that undergo an oxidation reaction with ANB

activate the FFGN. For the catalytic oxidation of ANB in the presence of H_2O_2, the removal efficiency was 56%. The mechanism of the oxidation was due to the H_2O_2 molecules that are absorbed on the surface of FFGN and are activated by the bounded Fe^{2+} and Fe^{3+} to generate $^{\bullet}OH$ radicals, which can catalyze the oxidation of ANB. The maximum degradation of 58% was obtained for the $Na_2S_2O_8$ oxidant, which is attributed to the generation of $SO_4{}^{2-}$, which serves as the driving force for the degradation of ANB [29]. Therefore, the effect of the concentration of $Na_2S_2O_8$ was performed to achieve better ANB degradation.

2.2.7. Effect of $Na_2S_2O_8$ Concentration

The effect of the $Na_2S_2O_8$ concentration on the degradation of ANB was performed by varying its concentration from 0.002 to 0.06 mol/L at the experimental conditions of pH = 3.0 ± 0.2, ANB = 50 ppm, FFGN = 0.5g/L, and T = 25 ± 1 °C. The degradation showed a drastic increase from 59% to 95% with an increase in the $Na_2S_2O_4$ concentration. The Fe_3O_4 present in the nanocomposites acts as an activator in the sulfate-radical-based AOP, and it initiates the electron mass transfer of the reacting species (ANB and $Na_2S_2O_8$), which may result in the formation of $SO_4{}^{-\bullet}$ radicals. These $SO_4{}^{-\bullet}$ radicals enhance the degradation of ANB.

$$S_2O_8^{2-} + e^- \rightarrow SO_4^{-\bullet} + SO_4^{2-} \quad (7)$$

$$ANB + SO_4^{-\bullet} \rightarrow [PNA]^{\bullet+} + SO_4^{2-} \quad (8)$$

The $S_2O_8{}^{2-}$ can be activated at the ferroferric oxide surface through electron transference to produce the sulfate radical that undergoes an oxidation reaction with ANB. The mechanism of the sulfate-radical-based AOP can be explained by the following reaction [29]:

$$S_2O_8^{2-} + Fe^{2+} \rightarrow Fe^{3+} + SO_4^{2-} + SO_4^{-\bullet} \quad (9)$$

$$SO_4^{-\bullet} + Fe^{2+} \rightarrow Fe^{3+} + SO_4^{2-} \quad (10)$$

$$SO_4^{-\bullet} + S_2O_8^{2-} \rightarrow SO_4^{2-} + S_2O_8^{-} \quad (11)$$

$$SO_4^{-\bullet} + SO_4^{-\bullet} \rightarrow S_2O_8^{2-} \quad (12)$$

$$SO_4^{-\bullet} + H_2O \rightarrow SO_4^{2-} + {}^{\bullet}OH + H^+ \quad (13)$$

$$SO_4^{-\bullet} + OH^- \rightarrow SO_4^{2-} + {}^{\bullet}OH \quad (14)$$

$$S_2O_8^{2-} + OH^- \rightarrow HSO_4^- + SO_4^{-\bullet} + 1/2O_2 \quad (15)$$

$$SO_4^{-\bullet} + H_2O \rightarrow HSO_4^- + {}^{\bullet}OH \quad (16)$$

To provide a reasonable comparison between the traditional Fenton process and the activated sulfate-radical-based Fenton oxidation process, the same pH was used. When compared to the traditional Fenton oxidation process, the sulfate-radical-based oxidation process was effective for the degradation of ANB based on the results obtained. The obtained degradation efficiency of the pollutant was compared with the reported literature, and the same was presented in Table 1. It was understood that the present catalytic study provides comparative superior degradation efficiency when compared to the reported literature; although, a direct comparison could not be performed as the catalyst synthesis procedure and degradation study conditions were different.

Table 1. Comparative results of 1-amino-nitrobenzene (ANB) degradation with the reported literature.

Catalyst Synthesis	Degradation Method	Degradation Efficiency	Reference
$AgBiO_3$ photocatalyst by Ion exchange followed by hydrothermal treatment	Photocatalytic degradation, reaction temperature 25 °C, 4-NP with initial concentration of 20 ppm, 5 h	90% removal with catalyst loading of 0.3 g/L	Boruah et al., 2019 [53]
Carbon nanotube-containing cathode	Heterogeneous electro-Fenton-like oxidation, 200 mL 4-nitrophenol (100 mg L^{-1}) solution containing Na_2SO_4 (0.10 M) with pH 3.0, 3.0 V (75 mA of average current), 240 min	100% removal with 10.0 g catalyst amount	Chu et al., 2020 [54]
In_2S_3/α-Fe_2O_3 composites by hydrothermal treatment	4-nitrophenol (20 mg/L), Visible light irradiation by a xenon lamp with a 420 nm filter, 0.05 g In_2S_3/α-Fe_2O_3, 50 mL reaction volume	95% of PNP was removed using the 60% In_2S_3/α-Fe_2O_3 catalyst after 100 min, 8% and 20% of PNP were degraded using the pure α-Fe_2O_3 and In_2S_3	Fang et al., 2021 [55]
Porous PbO_2-CNTs electrode was prepared by oxygen bubble template method	Electrocatalytic degradation, p-nitrophenol concentration of 50 mg·L^{-1} and 0.25 mol·L^{-1} Na_2SO_4, Electrode working area is 2 cm^2, current density of 30 mA·cm^{-2}, temperature of 30 °C, 120 min	96%—3D PbO_2-CNTs electrode, 85.2%—3D PbO_2, 86.4%—flat PbO_2-CNTs electrodes	You et al., 2021 [56]
Silver/carbon co-decorated hollow TiO_2 photocatalyst (Ag/C-TiO_2) by depositing Ag NPs on the surface of carbon decorated hollow TiO_2 sphere	Ag/C-TiO_2 (10 mg in 50 mL), 4-NP (10 mg/L), simulated sunlight irradiation (300 W Xe lamp equipped with an AM 1.5 filter), 60 min	Complete removal for the Ag/C-TiO_2 photocatalyst, 86% removal of 4-NP for C-TiO_2	Zhang et al., 2022 [57]
Natural polymer-based iron oxide (Fe_3O_4) nanocomposites by sonochemical precipitation method	pH = 3.0 ± 0.2, ANB = 50 ppm, $Na_2S_2O_8$ = 0.06 mol/L, Amplitude = 40%, Ultrasound Probe = 25 mm, T = 25 ± 1 °C, UV light, 60 min	95% degradation efficiency	This study

2.2.8. Recycling Study

To evaluate the recycling of the used FFGN, FFGN was repeatedly used by maintaining the same experimental conditions for five times. After each degradation study, the FFGN was removed by centrifugation, rinsed with distilled water, and finally dried. The dried FFGN was used for the next batch experiment. Figure 8 shows that the ANB removal efficiency gradually decreased with recycling. The FFGN was used effectively for up to two cycles to activate the oxidant and degrade ANB.

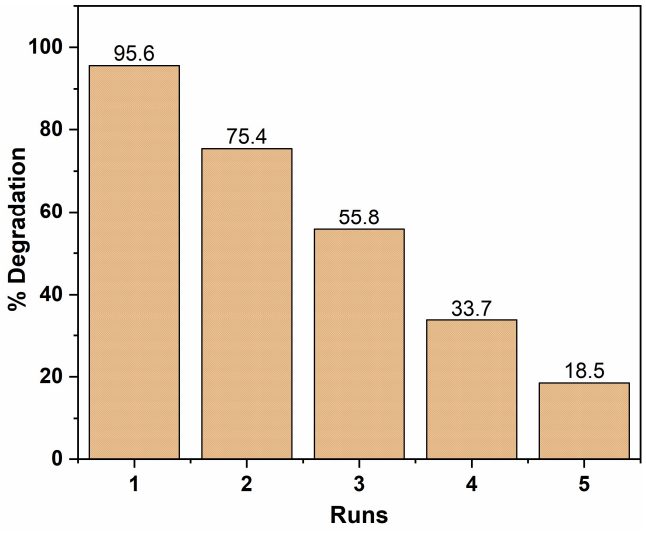

Figure 8. Recycling Study of FFGN for the catalytic oxidation of ANB (pH = 3.0 ± 0.2, ANB = 50 ppm, FFGN = 0.5 g/L, $Na_2S_2O_8$ = 0.06 mol/L, Amplitude = 40%, Probe = 25 mm, T = 25 ± 1 °C).

3. Materials and Methods

3.1. Materials

The chemicals that were used for nanocomposite synthesis and pollutant treatment were given as: Ferrous sulfate heptahydrate ($FeSO_4 \cdot 7H_2O$, Merck Life science Pvt Ltd.,

Mumbai, India), ethanol (C_2H_5OH, Changshu Hongsheng Fine Chemicals Co. Ltd., Changshu, China), sodium hydroxide (NaOH, Merck Life science Pvt Ltd., Mumbai, India), 1-amino-nitrobenzene ($C_6H_6N_2O_2$, Sisco Research Laboratories Pvt. Ltd., Mumbai, India), sodium metaperiodate ($NaIO_4$, Sisco Research Laboratories Pvt. Ltd., Mumbai, India), hydrogen peroxide (H_2O_2, Merck Life science Pvt Ltd., Mumbai, India), sodium persulphate ($Na_2S_2O_8$, Lobachemie, Mumbai, India), sulfuric acid (H_2SO_4, Merck Life science Pvt Ltd., Mumbai, India), guaran (Himedia Laboratories Pvt Ltd., Mumbai, India). Guaran is a constituent of Leguminosae family a galactomannan isolated from the seeds of *Cyamopsis tetragonolobus* [40] consisting of a linear backbone of D-mannopyranosyl backbone (β-1→4 glycosidic linkage) along with D-galactopyranosyl side branching (α-1→6 glycosidic linkages), at average galactose-to-mannose ratios of 1:1.6–1:2 [58]. Commercial guaran was supplied by Himedia (Himedia Laboratories Pvt Ltd., Mumbai, India) with a molecular weight M_w of 3.0×10^6 g/mol. The galactomannan ratio of ≥70%, protein content of ≤10%, sulfated ash of ≤1.5%, acid insoluble matter of ≤7.0%, and moisture content of ≤15% was present in the guaran. The ultrasonic processor (Sonics Vibra cell, VCX 500 Sonics and Materials Inc, Newtown, CT, USA) possess a horn tip of 13 mm diameter, operating frequency of 20 kHz, and the power was 500 W.

3.2. Ferroferric Oxide-Guaran Nanocomposite Synthesis

In order to synthesize Ferroferric oxide-Guaran nanocomposite (FFGN), a polymer material Guaran in hydrolyzed form was used as a substrate. Typically, to the 100 mL of 1 M $FeSO_4 \cdot 7H_2O$, the required quantity of 3 M NaOH was injected and ultrasonication was performed using an ultrasonic processor with an amplitude of 40% (i.e., 200 W). Then, the hydrolyzed Guaran (0.1 g/L) was added to the mixture and the reaction was performed in nitrogen atmosphere to prevent any reaction with atmospheric oxygen. The ultrasonication was passed until the complete formation of ferroferric oxide, which was indicated by the change in the color of the solution to black. The formed nanocomposite was washed to remove any impurities present using double distilled water and then dried under vacuum.

3.3. Degradation Study

A 500 mL cylindrical jacketed reactor was used to perform ANB degradation studies with cooling water circulation to continuously remove the heat and keep the temperature of the reaction solution steady. From the ANB stock solution, appropriate quantity was taken and diluted with deionized water to 200 mL to obtain the derived ANB concentration. The pH of the solution was adjusted using either sulfuric acid (0.1 M) or sodium hydroxide (0.1 M). The degradation study was carried out using an ultrasonic processor with 25 mm diameter probe and 200 W set power in the presence of ultraviolet light. The study was conducted for 120 min and change in concentration of ANB during this period was examined by taking samples every 15 min time interval. The degradation of ANB was performed with different oxidants such as sodium periodate ($NaIO_4$), sodium sulfate (Na_2SO_4), hydrogen peroxide (H_2O_2), and Sodium Persulfate ($Na_2S_2O_8$), respectively. The effects of initial pH, nanocomposite dose, 1-amino-nitrobenzene concentration, and oxidants concentration were studied. The change in the concentration of the ANB was evaluated from the absorbance value of the ANB aqueous solution obtained from the UV–vis spectrophotometer with the calibration curve.

3.4. Characterization and Analytical Techniques

The X-ray diffractometer (XRD, Ultima IV, Rigaku, Japan) of the nanocomposite was analyzed with Cu Kα radiation (k = 1.540562 Å, 2θ = 20° to 80°, scan speed = 1°/min, step size = 0.05°, voltage = 40 kV, current = 300 mA). The zeta potential of the nanocomposite was recorded using Malvern Zetasizer Nano-S (Malvern Instruments, Royston, United Kingdom). The morphology of the nanocomposite was studied using scanning electron microscopy (SEM) with Zeiss Zigma, Gottingen, Germany (resolution = 1.3 nm at 20 kV, acceleration voltage = 0.1–30 kV, magnification = 12–1 Mx). Transmission electron microscopy

(HRTEM- FEI Tecnai F20 S/TEM, Oregon, Hillsboro, OR, USA) was used to visualize the size, shape, and aggregation of nanocomposites. The UV–vis spectrophotometer was utilized to observe the change in ANB concentration with Shimadzu UV2600, Kyoto, Japan. The ANB showed the maximum absorbance wavelength (λ_{max}) at 380 nm. Therefore, the concentrations of the ANB in the reaction mixture at different reaction times were determined by measuring the absorption intensity at λ-max (380 nm).

4. Conclusions

The present study reported the green synthesis of ferroferric oxide nanocomposites using ultrasound. The TEM and SEM images showed that the synthesized nanocomposites are cubic in shape with a medium particle size of 47 nm. The sonophotochemical degradation of 1-amino-nitrobenzene (ANB) by the Fenton-like process significantly influenced the initial solution pH, $NaIO_4$ concentration, FFGN dosage, and initial ANB concentration. Degradation efficiency of 75% was obtained with FFGN along with $NaIO_4$ as the oxidant. However, a large quantity of FFGN was required. The sulfate-radical-based oxidation process has many advantages such as being more selective and having a longer lifetime compared to the $^{\bullet}OH$ radical. Under the optimum condition where pH = 3.0 ± 0.2, ANB = 50 ppm, $Na_2S_2O_8$ = 0.06 mol/L, Amplitude = 40%, Probe = 25 mm, and T = 25 ± 1 °C, the degradation efficiency was 95%. From the above-mentioned findings, it was evident that the sulfate-radical-based Fenton-oxidation process exhibited higher removal efficiency compared to the simple Fenton-oxidation process.

Author Contributions: M.K.: Synthesis, Degradation study. J.B.: Methodology, Material Characterization, Writing, Data Curation. T.S.: Methodology, Data Validation, Reviewing, Editing, Supervision. M.S.: Review and Editing. All authors have read and agreed to the published version of the manuscript.

Funding: The authors would like to thank National Institute of Technology, Tiruchirappalli, India for providing the required facilities to execute this research work. J. Balachandramohan would like to express his sincere gratitude towards the institute fellowship provided by the Ministry of Human Resource and Development, Government of India.

Data Availability Statement: The data presented in this study are available on request from the corresponding author.

Acknowledgments: The authors sincerely thank NIT Tiruchirappalli for providing the required facilities to complete this research work.

Conflicts of Interest: The authors declare no conflict of interest.

References

1. Shanker, V.; Rayabandla, S.M.; Kumavath, R.N.; Chintalapati, S.; Chintalapati, R. Light-Dependent Transformation of Aniline to Indole Esters by the Purple Bacterium Rhodobacter sphaeroides OU5. *Curr. Microbiol.* **2006**, *52*, 413–417. [CrossRef]
2. Travis, A.S. Manufacture and uses of the Anilines: A Vast Array of Processes and Products. *Chem. Anilines.* **2007**, 715–782. [CrossRef]
3. Kavitha, E.; Sundaraganesan, N.; Sebastian, S. Molecular structure, vibrational spectroscopic and HOMO, LUMO studies of 4-nitroaniline by density functional method. *Indian J. Pure. Appl. Phys.* **2010**, *48*, 20–30.
4. Oturan, M.A.; Peiroten, J.; Chartrin, P.; Acher, A.J. Complete Destruction of p -Nitrophenol in Aqueous Medium by Electro-Fenton Method. *Environ. Sci. Technol.* **2000**, *34*, 3474–3479. [CrossRef]
5. Sun, J.-H.; Sun, S.-P.; Fan, M.; Guo, H.-Q.; Lee, Y.-F.; Sun, R.-X. Oxidative decomposition of p-nitroaniline in water by solar photo-Fenton advanced oxidation process. *J. Hazard. Mater.* **2008**, *153*, 187–193. [CrossRef]
6. Ma, H.; Yao, S.; Zhang, J.; Pu, C.; Zhao, S.; Wang, M.; Xiong, J. Steady-state and transient photolysis of p-nitroaniline in acetonitrile. *J. Photochem. Photobiol. A Chem.* **2009**, *202*, 67–73. [CrossRef]
7. Wang, Y.; Zhang, Y.-N.; Zhao, G.; Wu, M.; Li, M.; Li, D.; Zhang, Y.; Zhang, Y. Electrosorptive photocatalytic degradation of highly concentrated p-nitroaniline with TiO_2 nanorod-clusters/carbon aerogel electrode under visible light. *Sep. Purif. Technol.* **2013**, *104*, 229–237. [CrossRef]
8. Khalid, A.; Arshad, M.; Crowley, D.E. Biodegradation potential of pure and mixed bacterial cultures for removal of 4-nitroaniline from textile dye wastewater. *Water Res.* **2009**, *43*, 1110–1116. [CrossRef]

9. Reddy, V.; Torati, R.S.; Oh, S.; Kim, C. Biosynthesis of Gold Nanoparticles Assisted by Sapindus mukorossi Gaertn. Fruit Pericarp and Their Catalytic Application for the Reduction of p-Nitroaniline. *Ind. Eng. Chem. Res.* **2013**, *52*, 556–564. [CrossRef]
10. Lee, D.S.; Park, K.S.; Nam, Y.W.; Kim, Y.-C.; Lee, C.H. Hydrothermal decomposition and oxidation of p-nitroaniline in supercritical water. *J. Hazard. Mater.* **1997**, *56*, 247–256. [CrossRef]
11. Sun, J.-H.; Sun, S.-P.; Fan, M.-H.; Guo, H.-Q.; Qiao, L.-P.; Sun, R.-X. A kinetic study on the degradation of p-nitroaniline by Fenton oxidation process. *J. Hazard. Mater.* **2007**, *148*, 172–177. [CrossRef] [PubMed]
12. Gautam, S.; Kamble, S.P.; Sawant, S.B.; Pangarkar, V.G. Photocatalytic degradation of 4-nitroaniline using solar and artificial UV radiation. *Chem. Eng. J.* **2005**, *110*, 129–137. [CrossRef]
13. Saupe, A. High-rate biodegradation of 3- and 4-nitroaniline. *Chemosphere* **1999**, *39*, 2325–2346. [CrossRef]
14. Zheng, K.; Pan, B.; Zhang, Q.; Zhang, W.; Pan, B.; Han, Y.; Zhang, Q.; Wei, D.; Xu, Z.; Zhang, Q. Enhanced adsorption of p-nitroaniline from water by a carboxylated polymeric adsorbent. *Sep. Purif. Technol.* **2007**, *57*, 250–256. [CrossRef]
15. Li, K.; Zheng, Z.; Feng, J.; Zhang, J.; Luo, X.; Zhao, G.; Huang, X. Adsorption of p-nitroaniline from aqueous solutions onto activated carbon fiber prepared from cotton stalk. *J. Hazard. Mater.* **2009**, *166*, 1180–1185. [CrossRef] [PubMed]
16. Wu, W.; Liang, S.; Chen, Y.; Shen, L.; Zheng, H.; Wu, L. High efficient photocatalytic reduction of 4-nitroaniline to p-phenylenediamine over microcrystalline $SrBi_2Nb_2O_9$. *Catal. Commun.* **2012**, *17*, 39–42. [CrossRef]
17. Wu, W.; Liu, G.; Liang, S.; Chen, Y.; Shen, L.; Zheng, H.; Yuan, R.; Hou, Y.; Wu, L. Efficient visible-light-induced photocatalytic reduction of 4-nitroaniline to p-phenylenediamine over nanocrystalline $PbBi_2Nb_2O_9$. *J. Catal.* **2012**, *290*, 13–17. [CrossRef]
18. Wu, W.; Wen, L.; Shen, L.; Liang, R.; Yuan, R.; Wu, L. A new insight into the photocatalytic reduction of 4-nitroaniline to p-phenylenediamine in the presence of alcohols. *Appl. Catal. B Environ.* **2012**, *130–131*, 163–167. [CrossRef]
19. Suslick, K.S. The Chemical Effects of Ultrasound. *Sci. Am.* **1989**, *260*, 80–86. [CrossRef]
20. Shirgaonkar, I.Z.; Pandit, A.B. Sonophotochemical destruction of aqueous solution of 2,4,6-trichlorophenol. *Ultrason. Sonochem.* **1998**, *5*, 53–61. [CrossRef]
21. Kritikos, D.E.; Xekoukoulotakis, N.P.; Psillakis, E.; Mantzavinos, D. Photocatalytic degradation of reactive black 5 in aqueous solutions: Effect of operating conditions and coupling with ultrasound irradiation. *Water Res.* **2007**, *41*, 2236–2246. [CrossRef] [PubMed]
22. Bejarano-Perez, N.J.; Suarez-Herrera, M.F. Sonophotocatalytic degradation of congo red and methyl orange in the presence of TiO_2 as a catalyst. *Ultrason. Sonochem.* **2007**, *14*, 589–595. [CrossRef] [PubMed]
23. Joseph, C.G.; Li Puma, G.; Bono, A.; Krishnaiah, D. Sonophotocatalysis in advanced oxidation process: A short review. *Ultrason. Sonochem.* **2009**, *16*, 583–589. [CrossRef]
24. Pizzigallo, M.D.R.; Ruggiero, P.; Crecchio, C.; Mascolo, G. Oxidation of Chloroanilines at Metal Oxide Surfaces. *J. Agric. Food Chem.* **1998**, *46*, 2049–2054. [CrossRef]
25. Phu, N.H.; Hoa, T.T.K.; Van Tan, N.; Thang, H.V.; Le Ha, P. Characterization and activity of Fe-ZSM-5 catalysts for the total oxidation of phenol in aqueous solutions. *Appl. Catal. B Environ.* **2001**, *34*, 267–275. [CrossRef]
26. Han, Y.-F.; Phonthammachai, N.; Ramesh, K.; Zhong, Z.; White, T. Removing Organic Compounds from Aqueous Medium via Wet Peroxidation by Gold Catalysts. *Environ. Sci. Technol.* **2007**, *42*, 908–912. [CrossRef] [PubMed]
27. Zelmanov, G.; Semiat, R. Iron(3) oxide-based nanoparticles as catalysts in advanced organic aqueous oxidation. *Water Res.* **2008**, *42*, 492–498. [CrossRef] [PubMed]
28. Ma, H.; Wang, M.; Pu, C.; Zhang, J.; Zhao, S.; Yao, S.; Xiong, J. Transient and steady-state photolysis of p-nitroaniline in aqueous solution. *J. Hazard. Mater.* **2009**, *165*, 867–873. [CrossRef] [PubMed]
29. Zhao, Y.S.; Sun, C.; Sun, J.Q.; Zhou, R. Kinetic modeling and efficiency of sulfate radical-based oxidation to remove p-nitroaniline from wastewater by persulfate/Fe_3O_4 nanoparticles process. *Sep. Purif. Technol.* **2015**, *142*, 182–188. [CrossRef]
30. Khan, I.; Zada, N.; Khan, I.; Sadiq, M.; Saeed, K. Enhancement of photocatalytic potential and recoverability of Fe_3O_4 nanoparticles by decorating over monoclinic zirconia. *J. Environ. Health Sci. Eng.* **2020**, *18*, 1473–1489. [CrossRef]
31. Pandey, S.; Goswami, G.K.; Nanda, K.K. Green synthesis of polysaccharide/gold nanoparticle nanocomposite: An efficient ammonia sensor. *Carbohydr. Polym.* **2013**, *94*, 229–234. [CrossRef]
32. Pandey, S.; Son, N.; Kim, S.; Balakrishnan, D.; Kang, M. Locust Bean gum-based hydrogels embedded magnetic iron oxide nanoparticles nanocomposite: Advanced materials for environmental and energy applications. *Environ. Res.* **2022**, *214*, 114000. [CrossRef] [PubMed]
33. Das, T.; Yeasmin, S.; Khatua, S.; Acharyab, K.; Bandyopadhyay, A. Influence of a blend of guar gum and poly(vinyl alcohol) on long term stability, and antibacterial and antioxidant efficacies of silver nanoparticles. *RSC Adv.* **2015**, *5*, 54059. [CrossRef]
34. Sharma, G.; Kumar, A.; Sharma, S.; Al-Muhtaseb, A.H.; Naushad, M.; Ghfar, A.A.; Ahamad, T.; Stadler, F.J. Fabrication and characterization of novel Fe0@Guar gum-crosslinked-soya lecithin nanocomposite hydrogel for photocatalytic degradation of methyl violet dye. *Sep. Purif. Technol.* **2019**, *211*, 895–908. [CrossRef]
35. Mathur, N.K. *Industrial Galactomannan Polysaccharides*; CRC Press Taylor & Francis Group: Boca Raton, FL, USA, 2012.
36. Busch, V.M.; Loosli, F.; Santagapita, P.R.; Buera, M.P.; Stoll, S. Formation of complexes between hematite nanoparticles and a non-conventional galactomannan gum. *Toward a better understanding on interaction processes. Sci. Total Environ.* **2015**, *532*, 556–563.
37. Bocchinfuso, G.; Mazzuca, C.; Sandolo, C.; Margheritelli, S.; Alhaique, F.; Coviello, T.; Palleschi, A. Guar Gum and Scleroglucan Interactions with Borax: Experimental and Theoretical Studies of an Unexpected Similarity. *J. Phys. Chem. B* **2010**, *114*, 13059–13068. [CrossRef]

38. Kumar, A.; Aerry, S.; Saxena, A.; de, A.; Mozumdar, S. Copper nanoparticulates in Guar-gum: A recyclable catalytic system for the Huisgen [3 + 2]-cycloaddition of azides and alkynes without additives under ambient conditions. *Green Chem.* **2012**, *14*, 1298–1301. [CrossRef]
39. Tiraferri, A.; Chen, K.L.; Sethi, R.; Elimelech, M. Reduced aggregation and sedimentation of zero-valent iron nanoparticles in the presence of guar gum. *J. Colloid Interface Sci.* **2008**, *324*, 71–79. [CrossRef]
40. Balachandramohan, J.; Anandan, S.; Sivasankar, T. A simple approach for the sonochemical synthesis of Fe_3O_4-guargum nanocomposite and its catalytic reduction of p-nitroaniline. *Ultrason. Sonochem.* **2018**, *40*, 1–10. [CrossRef]
41. Nidhin, M.; Indumathy, R.; Sreeram, K.J.; Nair, B.U. Synthesis of iron oxide nanoparticles of narrow size distribution on polysaccharide templates. *Bull. Mater. Sci.* **2008**, *31*, 93–96. [CrossRef]
42. Pandey, S.; Goswami, G.K.; Nanda, K.K. Green synthesis of biopolymer–silver nanoparticle nanocomposite: An optical sensor for ammonia detection. *Int. J. Biol. Macromol.* **2012**, *51*, 583–589. [CrossRef] [PubMed]
43. Pandey, S.; Mishra, S.B. Catalytic reduction of p-nitrophenol by using platinum nanoparticles stabilised by guar gum. *Carbohydr. Polym.* **2014**, *113*, 525–531. [CrossRef] [PubMed]
44. Balachandramohan, J.; Sivasankar, T. Sonication-assisted synthesis of a new heterostructured schiff base ligand Silver-Guar gum encapsulated nanocomposite as a visible light photocatalyst. *J. Microencapsul.* **2020**, *37*, 29–40. [CrossRef]
45. Balachandramohan, J.; Sivasankar, T.; Sivakumar, M. Facile sonochemical synthesis of Ag_2O-guar gum nanocomposite as a visible light photocatalyst for the organic transformation reactions. *J. Hazard Mater.* **2020**, *385*, 121621. [CrossRef]
46. Amritha, A.S.; Manu, B. Low cost Fenton's oxidative degradation of 4-nitroaniline using iron from laterite. *Water Sci. Technol.* **2016**, *74*, 1919–1925. [CrossRef] [PubMed]
47. Remucal, C.K.; Sedlak, D.L. The Role of Iron Coordination in the Production of Reactive Oxidants from Ferrous Iron Oxidation by Oxygen and Hydrogen Peroxide. In *Aquatic Redox Chemistry*; ACS Symposium Series; Oxford University Press: New York, NY, USA, 2011; pp. 177–197.
48. Khan, I.; Saeed, K.; Ali, N.; Khan, I.; Zhang, B.; Sadiq, M. Heterogeneous photodegradation of industrial dyes: An insight to different mechanisms and rate affecting parameters. *J. Environ. Chem. Eng.* **2020**, *8*, 104364. [CrossRef]
49. Khan, I.; Saeed, K.; Zekker, I.; Zhang, B.; Hendi, A.H.; Ahmad, A.; Ahmad, S.; Zada, N.; Ahmad, H.; Shah, L.A.; et al. Review on Methylene Blue: Its Properties, Uses, Toxicity and Photodegradation. *Water* **2022**, *14*, 242. [CrossRef]
50. Ai, Z.; Yang, P.; Lu, X. Degradation of 4-chlorophenol by a microwave assisted photocatalysis method. *J. Hazard Mater.* **2005**, *124*, 147–152. [CrossRef]
51. Kutty, S.R.M.; Ngatenah, S.N.I.; Johan, N.A.; Amat, K.A.C. Removal of Zn (II), Cu (II), Chemical Oxygen Demand (COD) and Colour from Anaerobically Treated Palm Oil Mill Effluent (POME) using Microwave Incinerated Rice Husk Ash (MIRHA). *Int. Conf. Environ. Ind. Innov.* **2011**, *12*, 90–94.
52. Sanz, J.; De Luis, A.M.; Ortueta, M.; Varona, F.; Lombraña, J.I. Microwave and Fenton's reagent oxidation of wastewater. *Environ. Chem. Lett.* **2003**, *1*, 45–50. [CrossRef]
53. Ou, H.; Chen, Z.; Yu, Q.; Zhu, W.; Chen, B.; Lv, Z.; Hu, Q.; Liu, Y.; Zheng, Z.; Li, S.; et al. Preparation of a three-dimensional porous PbO_2-CNTs composite electrode and study of the degradation behavior of p-nitrophenol. *Sep. Purif. Technol.* **2021**, *276*, 119406. [CrossRef]
54. Zhang, Y.; Xiao, Y.; Liu, X.; Yin, Z.; Cao, S. Silver/carbon co-decorated hollow TiO_2 catalyst drives the efficient photocatalytic degradation/catalytic hydrogenation of 4-nitrophenol. *J. Taiwan Inst. Chem. Eng.* **2022**, *133*, 104274. [CrossRef]
55. Fang, L.; Jiang, R.; Zhang, Y.; Munthali, R.; Huang, X.; Wu, X.; Liu, Z. Enhanced photocatalytic activity for 4-nitrophenol degradation using visible-light-driven In_2S_3/α-Fe_2O_3 composite. *J. Solid State Chem.* **2021**, *303*, 122461. [CrossRef]
56. Chu, Y.; Miao, B.; Zhang, X.; Lv, R. Heterogeneous electro-Fenton-like oxidation for the degradation of 4-nitrophenol characterized by immobilized Fe(III): Performance, mechanism and chlorinated organic compounds formation. *J. Water Process. Eng.* **2020**, *38*, 101662. [CrossRef]
57. Boruah, B.; Gupta, R.; Modak, J.M.; Madras, G. Novel insights into the properties of $AgBiO_3$ photocatalyst and its application in immobilized state for 4-nitrophenol degradation and bacteria inactivation. *J. Photochem. Photobiol. A: Chem.* **2019**, *373*, 105–115. [CrossRef]
58. Balachandramohan, J.; Sivasankar, T. Ultrasound assisted synthesis of guar gum-zero valent iron nanocomposites as a novel catalyst for the treatment of pollutants. *Carbohydr. Polym.* **2018**, *199*, 41–50. [CrossRef]